Hydrogenation of Carbon Species on Cobalt Catalysts Observed by Raman–Ellipsometry Spectroscopy

MASAO WATANABE

Research Institute for Catalysis, Hokkaido University, Sapporo 060, Japan

A combined system of Raman spectroscopy and ellipsometry is developed for the observation of catalyst surfaces under reaction conditions. The deposition of carbon species on Co catalysts during the Boudouard reaction and the hydrogenation of these carbon species are observed quickly and *in situ* by a rotating analyzer ellipsometer in connection with the observation of Raman scattering of the surface carbon species and the mass analysis of the product. Prior to the hydrogenation reaction the state of surface hydrogen on Co was studied by the ellipsometer at temperatures above the desorption temperature T_d determined by TDS. It is concluded that hydrogen atoms on Co are mainly located at subsurface sites at $T > T_d$, and the surface carbons are attacked by them from the metal side to produce hydrocarbons. © 1988 Academic Press, Inc.

1. INTRODUCTION

Optical methods such as ellipsometry and Raman scattering as well as IR absorption are considered to be powerful for the analysis of surface properties and surface chemical species under normal/high gas pressures. We have developed a Raman-ellipsometry combined system with the use of the Ar laser light in an attempt to study *in situ* microscopic surface layers formed on Fe and Fe_3O_4 surfaces (*1, 2*). Ellipsometry is very sensitive to changes in surface properties of metals. It informs us of the dielectric function $\varepsilon = \varepsilon' - i\varepsilon''$ and thickness D of an adsorbed layer or a thin surface layer (*3, 4*). An automated rotating analyzer ellipsometer (*5*) is especially useful to follow rapid surface reactions. It takes about 0.1 sec for the ellipsometer to determine surface layer properties. The ellipsometric response is represented by two parameters of Δ and Ψ which are defined by

$$r_p/r_s = \tan \Psi \exp(i\Delta),$$

where r_p and r_s are the amplitude reflectance of *p*- and *s*-polarized light, respectively; Ψ is called the amplitude ratio; and Δ is the phase difference. Δ and Ψ observed from a clean surface determine the dielectric function of the bulk metal (*4*). A surface reaction may cause Δ and Ψ to vary owing to the formation of a surface layer or an adlayer, i.e., $\delta\Delta = \Delta(\text{clean}) - \Delta(\text{reacted})$, and $\delta\Psi = \Psi(\text{clean}) - \Psi(\text{reacted})$, from which one can determine the dielectric function of the layer and its thickness (*1–6*).

Raman spectroscopy, on the other hand, is insensitive to surface properties, but the SERS effect can be applied to study surface species. Graphite is known to be strongly surface enhanced on silver surfaces producing two broad Raman bands at 1340 and 1570 cm^{-1} (*7, 8*). We have found that surface graphite as thin as about 20 nm produced on Fe surfaces by the Boudouard reaction (B-reaction) (*9*), $2CO \rightarrow CO_2 + C_{ad}$, exhibits specific Raman bands at 1120 and 1150 cm^{-1} as well as the well-known bands at 1350 and 1580 cm^{-1} (*2*). The Raman scattering of graphite is the most helpful in the application of SERS to catalysis science.

In this paper we intend to exemplify the ellipsometric method applied to the observation of rapid changes in surface properties of Co catalysts during CO or H_2 adsorption and the hydrogenation reaction of surface carbon species at high temperatures under ambient gas phase. Cobalt is a good

catalyst for the F–T synthesis reaction (10), but its surface and adsorbative properties are not well understood due to the phase transition at 430°C. CO gas is adsorbed associatively on (0001) and (1010) surfaces but adsorbed dissociatively on (1120), (1012), and polycrystalline surfaces (11–13). The F–T reaction produces hydrocarbons of C = 1–12, whose reaction is characterized to be structure sensitive (14). The stability of surface carbon species such as CH and CH_2 was studied by Steinbach et al. and others with decomposing C_2H_4 and C_2H_2 molecules (15, 16). The above studies have aimed at characterizing carbon species on Co surfaces by means of AES, LEED, XPS, UPS, and TDS under high vacuum, which are unable to inform us of the state of surface hydrogen. In order to understand the mechanism of catalytic hydrogenation reactions, one must know the property of surface hydrogen. Zowtiak and Bartholomew (17) have observed a peculiar property of adsorbed hydrogen on Co by the TDS method. The peak temperature and the amount of ad-hydrogen depend strongly upon the adsorption temperature; the amount becomes maximum at the adsorption temperature about 100°C, and most of the ad-hydrogen is desorbed about 200°C. However, we often introduce hydrogen gas onto Co surfaces above 200°C to produce hydrocarbons. We are strongly conscious of the fact that high-vacuum surface science helps little in understanding catalytic reactions at high temperatures under ambient gas phase.

Reported here is a new approach to analyzing catalyst surfaces optically under ambient gas phase. In Section 3, after a description of experimental methods in Section 2, the ellipsometric method is explained; it requires complicated computer calculations to deduce useful surface layer parameters from observed ellipsometric angles. In Sections 4.1 and 4.2 the accumulation of carbon species on Co during B-reaction observed by ellipsometry and the states of the surface carbon species ana-

lyzed by Raman scattering are discussed. In Sections 4.3 and 4.4 rapid dissociation reactions of H_2 molecules on Co as well as hydrogenation reactions of the surface carbon species are discussed according to the ellipsometric analysis. Finally a new reaction mechanism for the hydrogenation of the surface carbon species is proposed.

2. EXPERIMENTAL

The details of the experimental methods are given elsewhere (1, 2). The Raman–ellipsometry combined system is shown schematically in Fig. 1. A reaction-optics chamber was made of fused quartz without using any metal parts. It was connected to a UHV system which was equipped with gas sources and a quadrupole mass spectrometer. The Raman spectrometer was Ramanor HG-2S (Jobin Yvon). An Ar laser (1.5 W, λ = 514.5 nm) was used as the light source. The light intensity was 100 to 300 mW at the sample surface. The rotating analyzer ellipsometer was designed according to the method by Hauge and Dill (18). Δ and Ψ were determined in 75 msec. However, very precise observations for small changes in $\delta\Delta$ and $\delta\Psi$ were performed by accumulating and averaging the signals for 1 sec. All the ellipsometric results presented here were obtained in this manner. The incident angle of the light was 70°.

The Co metal samples were polycrystalline plates (99.99%, 20 × 20 × 1 mm), which were at first polished electrochemically in phosphoric acid, then decarbonized in a flow of (H_2 + H_2O) gas at 800°C for 1 day and successively at 400°C for 3 days, and further reduced at 400°C in a flow of H_2 gas for 3 days. X-ray diffraction indicated that the crystal was in purely hcp structure. Each of the samples was sealed in a glass tube in N_2 atmosphere, which was then transferred to an AES analyzer (ANELVA, AAS-200). Auger spectra of a slowly air-contacted Co sample are shown in Fig. 2 with and without an Ar bombardment (3.0 kV, p(Ar) = 5 × 10^{-5} Torr). Spectrum (a) without the bombardment indicates the ex-
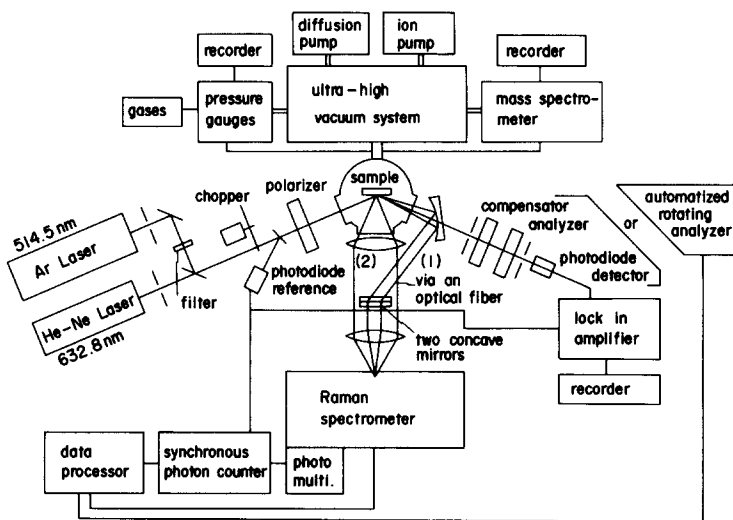
FIG. 1. Schematic illustration of the Laser Raman–ellipsometry combined system. Manual type and rotating analyzer ellipsometers are installed in the system.

istence of a large amount of Cl and C contaminants. Spectrum (b) after the bombardment for 1 min reveals the disappearance of the Cl and C impurities indicating that they are mainly originated from the contact with air and the glass wall when the sample was sealed in a glass tube and transferred to the Auger chamber. The Ar-bombarded sample was quickly set in the reaction-optics chamber in a flow of He gas. After the evacuation it was again reduced at 400°C in H_2 gas. Although we could not analyze surface impurities under working conditions, we were convinced that the surface of our samples was fairly clean with about 10% of C and S

impurities on the surface. It was found that the ellipsometric responses to the gas reactions became dull, small, and irreducible, when the surface was contaminated. CO gas was directly supplied from a highly pure CO cylinder containing 99.9999% pure CO gas. H_2 gas was purified by an H_2 purifier using a Pd–Ag capillary. The mass spectrometer indicated no trace of impurities in the gases within its sensitivity.

3. ANALYSIS OF ELLIPSOMETRIC RESPONSES

It may be convenient to show simultaneously experimental results and results of
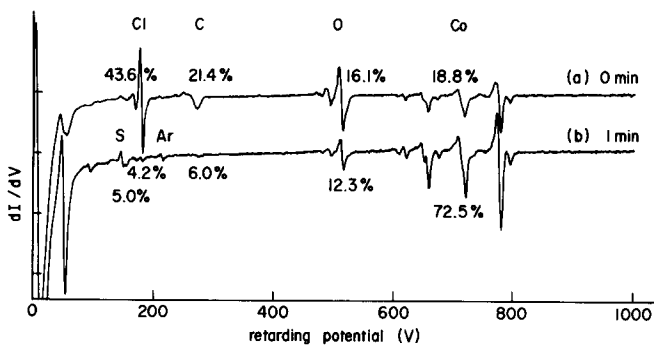
FIG. 2. Auger spectra of a Co sample contacted slowly with air. (a) Evacuated at 23°C. (b) Evacuated at 23°C and Ar-bombarded (3.0 kV, 5×10^{-5} Torr) for 1 min.
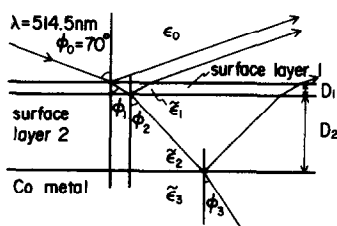
FIG. 3. Stratified layer model for the analysis of observed $\delta\Delta$ and $\delta\Psi$, and the definition of layer parameters.

the analysis, because observed ellipsometric parameters indicate less intuitively what is happening on the surface. Changes in ellipsometric angles $\delta\Delta$ and $\delta\Psi$ can be analyzed by the classical stratified layer model (3, 6, 19) shown in Fig. 3, where surface layers are separated by hypothetically sharp boundaries and are assumed to be homogeneous and isotropic. The interactions between the two layers or between the lower layer and the substrate are ignored. However, effects of the interaction are included effectively in the modification of the dielectric functions. The evaluated dielectric functions of the layers are thus apparent according to this model and differ to some extent from true ones. This model is reasonable for more than 10 thick surface layers, in which effects of the boundaries are negligible for the most part. However, the above classical model involves serious problems of nonclassical surface reflectance for monolayer adsorption on metal surfaces (20, 21). In the classical layer model observed Δ and Ψ are expressed by the set of classical Fresnel equations together with the Snell law as a function of the dieletric functions and the thickness of each layer and the substrate (4, 19). The analysis requires computer calculations because the dielectric functions are complex and the refraction angles become accordingly complex. Mathematical formulas are given in Refs. (3, 6, 19). When $D_1 \ll D_2$ (neglection of the D_1 layer) and the incident wavelength is $\lambda \gg D_2$, $\delta\Delta$ and $\delta\Psi$ due to the formation of the D_2 layer are expressed by

simple analytical forms taking only the first-order term of D_2/λ in an expanded series expression of the reflectance, which is called the linear approximation. This method is discussed in Refs. (3, 4). In this case we have three parameters, ε_2', ε_2'', and D_2, to be determined, whereas we have only two observations, $\delta\Delta$ and $\delta\Psi$. This problem is treated in detail in Ref. (1). The essential point in determining the three parameters is that $\delta\Delta$ and $\delta\Psi$ are the imaginary and real parts of the ellipsometric function, respectively, which are related to one another by the Kramers–Kroenig relations. $\delta\Delta$ and $\delta\Psi$ are hence not independent and the ratio $\delta\Delta/\delta\Psi$, which is independent of D_2 in the linear approximation, is prescribed to be a certain value by the spectroscopic optical properties of the layer and the metal substrate. In consequence, the three unknown parameters are uniquely determined by observed $\delta\Delta$ and $\delta\Psi$ with the supplementary condition $\delta\Delta/\delta\Psi$. For instance, $\delta\Delta/\delta\Psi$ is -2.1 at stage (1) in Fig. 4 for the CO reaction, which, its sign in par-
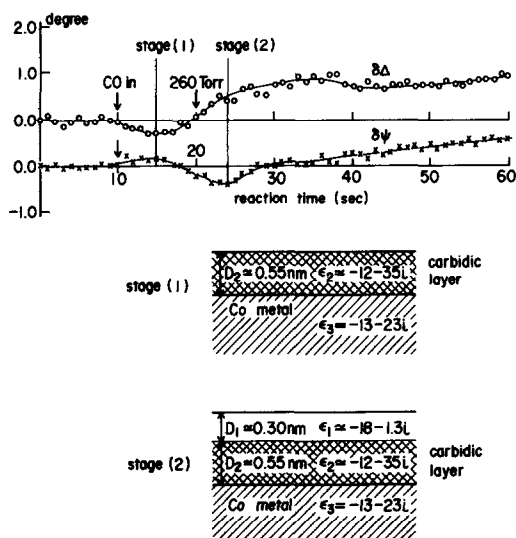
FIG. 4. Ellipsometric response to the reaction of CO gas on Co at 230°C, and results of the layer model analysis at stages (1) and (2). The scatterings of $\delta\Delta$ and $\delta\Psi$ within the initial 10 sec are caused by mechanical shocks as a leak valve is driven. Note that the CO pressure is steady after about 20 sec.
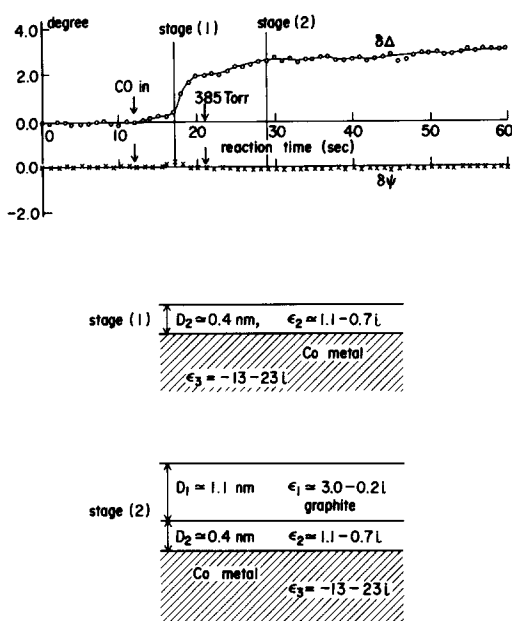
FIG. 5. Ellipsometric response to the reaction of CO gas on Co at 400°C, and results of the layer model analysis at stages (1) and (2). The CO pressure becomes steady after 21 sec.

ticular, severely restricts the choice of ε_2' and ε_2'' values in practice.

When a new D_1 layer is formed on the D_2 layer, the same method is applicable with the approximation that the D_1 layer is formed on a modified substrate with an effective dielectric function determined by ε_2, D_2, and ε_3, which is actually observed before D_1 is formed, and easily calculated by the layer model.

4. RESULTS AND DISCUSSIONS

4.1. Boudouard Reaction on Cobalt

Nakamura et al. (22) report that the state of carbon species on cobalt produced by B-reaction at 230°C is different from that produced at 400°C. This fact is confirmed by the results shown in Figs. 4 and 5, where ellipsometric responses to B-reaction at 230 and 400°C are presented as a function of reaction time. The occurrence of B-reaction is ascertained by observing CO_2 production in gas phase during the CO reaction. At about 10 sec CO gas begins to be

introduced; the pressure rises rapidly and after about 20 sec it becomes constant at 260 Torr in this case. It is necessary to remark that a small temperature effect is involved in this result, because cold CO gas (23°C) is suddenly introduced to the hot cobalt surface. In order to compensate for this cooling effect, the heater current is increased prior to the gas dosage, but there are minor effects on $\delta\Delta$ ($\sim0.1°$) and $\delta\Psi$ ($\sim0.05°$), which are small as seen by scatterings of $\delta\Delta$ and $\delta\Psi$ in Figs. 4 and 5, caused by mechanical shocks as a leak valve is driven. Similar scatterings are seen in other ellipsometric data within 10 to 12 sec before the gas dosage.

It may be instructive to give intuitive and qualitative explanations of $\delta\Delta$ and $\delta\Psi$ observed from metal surfaces. Positive $\delta\Delta$ signifies an accumulation of some species on the surface, while negative $\delta\Delta$ signifies either an elimination of a surface layer or often an absorption of gases into metals. The meaning of $\delta\Psi$ is complicated. When a strongly absorbative surface layer ($\varepsilon'' \gg 1$) is formed, or when the metal surface is strongly modified by a surface reaction, $\delta\Psi$ varies positively or negatively depending upon dielectric functions of the surface layer and the metal (19, 23). Weak adsorption of gases induces negligibly small and negative $\delta\Psi$ (3, 24). Based upon the above explanations the result at 230°C may be interpreted as the formation of a carbidic layer in the Co metal because of the negative $\delta\Delta$ at stage (1), whereas the result at 400°C may be interpreted as the formation of a graphite layer because of the large positive $\delta\Delta$ and the very small and negative $\delta\Psi$ at stage (2).

The observed $\delta\Delta$ and $\delta\Psi$ at stages (1) and (2) in Figs. 4 and 5 are analyzed by the stratified layer model discussed in the preceding section, whose results are shown at the bottom of Figs. 4 and 5. It is noted in Fig. 4 that the carbidic layer in D_2 is still metallic with the negative real part, and the D_1 layer on the D_2 layer may be another kind of carbide layer, but its property is un-
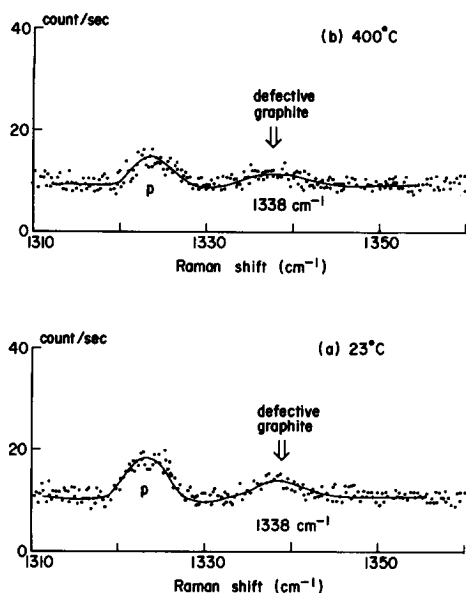
FIG. 6. Raman bands of surface defective graphite observed at (a) 23°C and (b) 400°C produced by B-reaction at 400°C. The property of the graphite is specified by the ellipsometric observation shown in Fig. 5. Peak p denotes a plasma emission from the Ar laser.

clear because of the very specific (but apparent) dielectric function. On the other hand, the dielectric functions of the probable surface graphite in Fig. 5 are found to be $\varepsilon_1 \simeq 3.0 - 0.2i$ and $\varepsilon_2 \simeq 1.1 - 0.7i$ in D_1 and D_2 layers, respectively, in comparison to that of the pyrolytic graphite, $\varepsilon = 2.81 - 1.10i$, which we observed. Noted in Fig. 5 is that the graphite formation is completed almost within 30 sec at 400°C, which is much faster than the reaction at 230°C. The thicknesses determined by the layer model analysis should be understood as averaged values, because actual distributions of the thickness are averaged out in the model. Ellipsometric information is thus macroscopic because of the macroscopic analysis, despite the ellipsometric response being in itself quite microscopic (23).

4.2. Raman Spectra of Surface Carbon Species

Since the ellipsometric observation determined the presence of surface graphite

produced by B-reaction at 400°C, we tried to detect its Raman bands. For a period of time we could find no band, but we finally succeeded in detecting three kinds of very weak Raman bands. Figure 6 shows that a Raman band at 1338 cm^{-1} appeared from the surface graphite shown in Fig. 5. The defective graphite in bulk is known to produce a band at 1340 cm^{-1} that is ascribed to the band from defective grain boundaries (25), so this band undoubtedly originates from the surface defective graphite. In Fig. 6 peaks denoted by p are plasma peaks emitted from the Ar laser, and so are meaningless. It is noted that the state of the graphite at 23°C is basically unchanged at 400°C, although its intensity becomes a little weak at 400°C. Furthermore, we could observe another Raman band at 1515 cm^{-1} from the same sample as that shown in Fig. 7, which can be attributed to amorphous graphite (26), whose intensity also becomes weaker at 400°C. We conclude therefore that defective graphite and amorphous graphite are produced on the Co surface by B-reaction at 400°C, which may exist as a
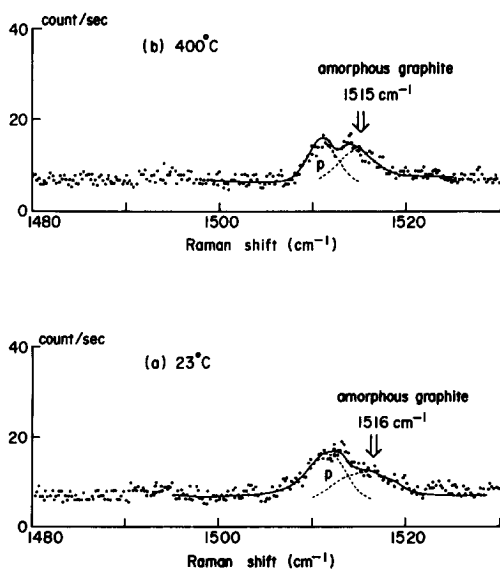
FIG. 7. Raman bands of surface amorphous graphite observed at (a) 23°C and (b) 400°C produced by B-reaction at 400°C. Peak p denotes a plasma emission from the Ar laser.
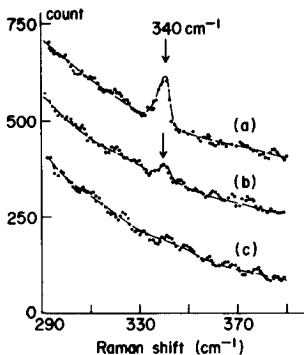
FIG. 8. Raman band at 340 cm^{-1} observed at 23°C. (a) After B-reaction at 230°C; the layer property is specified by the ellipsometric observation shown in Fig. 4. (b) After the hydrogenation reaction at 230°C. (c) After B-reaction at 400°C; no Raman band is seen in this wavenumber region.

mixture, because the observed dielectric function of the graphite layer is very different from that of pyrolytic graphite. Another important fact is that the intensities of the two Raman bands remain almost unchanged after the hydrogenation reaction (to be discussed later) indicating that those graphites contribute little to hydrocarbon production.

For the carbon species produced by B-reaction at 230°C a very weak Raman band at 340 cm^{-1} is observed as shown in Fig. 8, and is considered to be a vibrational mode of Co–C–Co (twofold bridged carbon species) (27). Curve (a) in Fig. 8 is observed from the surface layer shown in Fig. 4, which diminishes after the hydrogenation reaction in curve (b). Curve (c) exhibits no band after B-reaction at 400°C, indicating that a possible carbidic carbon species in the D_2 layer in Fig. 5 differs from those at 230°C as imagined from its dielectric function.

4.3. Adsorption of Hydrogen on Cobalt at 230 and 400°C

The state of hydrogen on the Co surface is studied using the same ellipsometric method to understand the mechanism of hydrogenation of the surface carbon species. Figures 9 and 10 demonstrate ellipsometric responses to the reaction of hydrogen with the pure Co surface at 230 and 400°C, respectively. Characteristic to the reaction time courses is that the initial negative $\delta\Delta$ (stage (1)) and the subsequent large

FIG. 9. Ellipsometric response to the reaction of hydrogen on the pure Co surface at 230°C, and results of the layer model analysis at stages (2) and (3). The origin of $\delta\Psi$ is conveniently shifted.
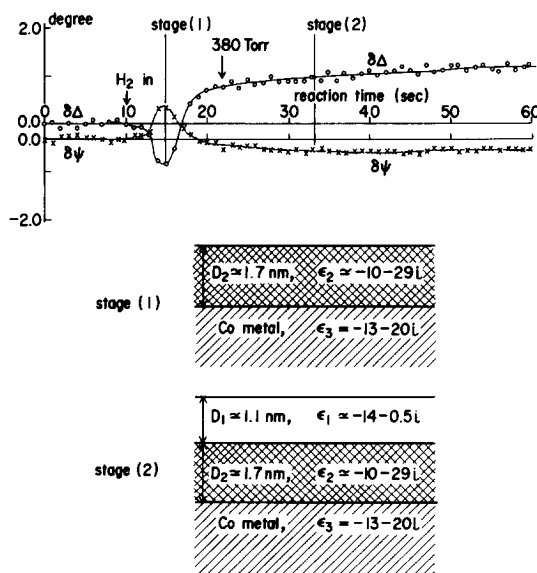
FIG. 10. Ellipsometric response to the reaction of hydrogen on the pure Co surface at 400°C, and results of the layer model analysis at stages (1) and (2).

and positive $\delta\Delta$ (stage (2)) are commonly observed at both temperatures. A multilayer adsorption of molecular hydrogen, if exists, is expected to produce $\delta\Delta \sim 0.5°$ and $\delta\Psi \sim 0.0°$ (28, 29), which are inconsistent with the observed variations. The layer model analysis results in the formation of surface layers shown at the bottom of Figs. 9 and 10. The state of hydrogen at stage (1) in Fig. 10 can be understood as dissolved and protonic hydrogen in a surface region of the Co whose thickness is concluded to be about 1.7 nm because of the negative $\delta\Delta$ and the metallic dielectric function. The state of hydrogen at stage (1) in Fig. 9 may be understood to be similarly dissolved hydrogen. However, the observed $\delta\Delta$ and $\delta\Psi$ are so small that the classical layer model analysis cannot be applied. Therefore, its layer parameters are undetermined in Fig. 9. The state of hydrogen in the D_1 layer at stages (2) and (3) in Fig. 9 is approximately determined by the layer model, neglecting the thin layer formed at stage (1). D_1 layers in Figs. 9 and 10 can be understood to be hydride-like layers on the layer of dissolved hydrogen. It is noted that the state of the hydride-like layer at stage (3) in Fig. 9 is considerably different from that at stage (2), possibly due to a higher concentration of hydrogen atoms in the Co metal.

The dielectric function of Co is expressed by

$$\varepsilon_3 = \varepsilon_f + \varepsilon_d + \varepsilon_i, \qquad (1)$$

where ε_f is the contribution from free electrons, ε_d is that from d electrons, and ε_i is that due to interband transitions. ε_f is given by the Drude equation

$$\varepsilon_f = \{1 - (\omega_p/\omega)^2\} - i(\omega_p/\omega)^2(\omega\tau)^{-1}, \qquad (2)$$

where ω is the frequency of the incident light and ω_p is the plasma frequency given by $\omega_p^2 = 4\pi Ne^2/m^*$. τ is the mean lifetime of free electrons. The negatively large real parts of ε_2 and ε_3 are understood by Eq. (2); further, the negative real parts in D_2 layers are interpreted in terms of changes in the number of free electrons, N, due to the protonic hydrogen (28); the large imaginary part of ε_2 in Fig. 10 is explainable with a shorter lifetime τ due to additional scatterings of free electrons by the dissolved protons in addition to a probable increase in the interband transitions in Eq. (1). The hydride-like layer at 400°C is more conductive than those at 230°C as indicated by the negatively large real part of the dielectric function.

The solubility of hydrogen in Co has been measured (30), but stable and bulk hydrides of Co have never been observed under normal pressure. Therefore, it seems that the hydride-like layers that we determined are specific to the surface, which cannot be detected by ordinary macroscopic observations of hydrogen absorption (31). We now realize that there are almost no molecular hydrogen and no atomic hydrogen adsorbed outside the Co surface at high temperatures above $T_d = 200°C$ even under ambient H_2 gas of 400 Torr: most hydrogen is located in the Co metal. As discussed in the Introduction, Zowtiak and Bartholomew (17) observed the peculiar thermal desorption spectra of hydrogen from polycrystalline Co surfaces, which they explained as an activated adsorption and desorption of hydrogen on Co surfaces. Their results seem to be consistent with the present ellipsometric data. The adsorbed hydrogen at an adsorption temperature of 200°C in their TDS experiments may correspond to the hydrogen in the D_2 layer. The subsurface hydrogen on Pd surfaces was studied in detail by Behm et al. (32), who found that it can easily come up to the surface even at room temperature.

4.4. Hydrogenation of Surface Carbon Species

The reactivity of the carbon species on the Co with H_2 gas is now studied using the ellipsometric method. The reaction time courses at 230 and 400°C are shown in Fig. 11 and the product of the reactions is shown in Fig. 12. The observed $\delta\Delta$ and $\delta\Psi$ are
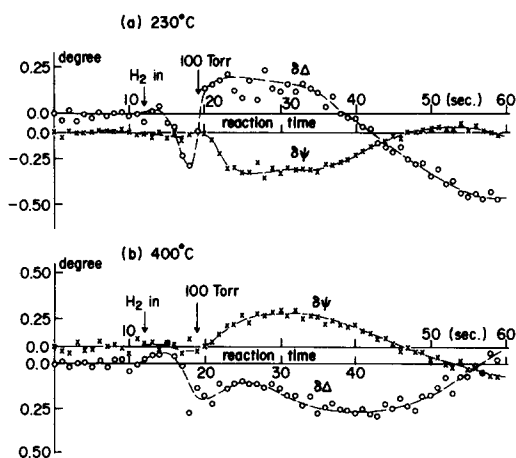
FIG. 11. Dynamical ellipsometric responses to the reaction of surface carbon species on Co with hydrogen gas (a) at 230°C and (b) at 400°C. The origin of $\delta\Psi$ is conveniently shifted.

complicated, so we try to explain them qualitatively. The reaction at 230°C may be understood as follows: the first large drop of $\delta\Delta$ at 17 sec is caused by absorption of hydrogen into the subsurface (dissolved hydrogen); the subsequent response is possibly due to the formation of CH compounds
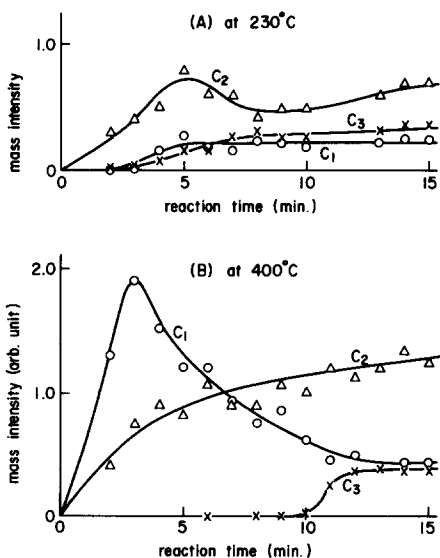
FIG. 12. Hydrocarbon productions by the reaction shown in Fig. 11 plotted against reaction time (A) at 230°C and (B) at 400°C.

on the surface inducing the positive $\delta\Delta$ at 20 to 33 sec. CH compounds can exist stably on the surface at 230°C (15). Then desorption of hydrocarbons takes place after 35 sec with decreasing $\delta\Delta$. The mass analysis in Fig. 12 in the gas phase reveals the main product of C_2 and C_3 hydrocarbons. There may be a small amount of heavier hydrocarbons but they are unclear in our mass analysis. Similarly at 400°C, hydrogen is at first absorbed into the subsurface, but CH compounds cannot be accumulated on the surface because of the high temperature (15). Some surface reactions occur on the surface inducing the positive $\delta\Psi$ during the production of hydrocarbons but they are unknown. The mass analysis indicates the production of C_1 and C_2 hydrocarbons at an early stage of the reaction, which suggests that the resident time of CH compounds on the surface seems to control the weight of hydrocarbons produced. There is no evidence showing the presence of a hydride-like layer, when the surface is covered with the carbon species.

Summarizing the reaction of the surface carbon species with hydrogen, it is very probable that the surface carbon is attacked by atomic hydrogen from the metal side, since the protonic hydrogen in the Co is expected to be more mobile, although we cannot deny minor hydrogenation mechanisms by hydrogen directly from the gas phase. If the Co surface is homogeneously covered with thick graphite at 400°C (see Fig. 5), hydrogen cannot be adsorbed and is absorbed to create the subsurface hydrogen. The graphite produced by B-reaction is expected to be heterogeneous on the polycrystalline Co surface. The hydrogenation of surface carbon species owes much to the heterogeneity on the surface.

5. CONCLUSION

The Raman–ellipsometry combined system is shown to be a powerful tool to study surface chemical reactions under reaction conditions. The Boudouard reaction and the hydrogenation of surface carbon spe-

cies are observed *in situ* by the rotating ana-
lyzer ellipsometer, which clarifies the pres-
ence of carbidic layers or graphite layers
and their properties.

It is concluded that the surface hydrogen
on Co at temperatures above T_d is mainly
located at subsurface sites in a protonic
state, which attacks very possibly the car-
bon species on the Co surface from the
metal side to produce hydrocarbons; the re-
action process is often stepwise in the time
scale of seconds, like an initial reaction to
produce the subsurface hydrogen, the next
reaction to produce CH compounds on the
surface, and then the desorption of hydro-
carbons. Surface reactions are thus unex-
pectedly slow to provide preferable circum-
stances at each step of the chemical
reactions.

ACKNOWLEDGMENTS

REFERENCES

1. Watanabe, M., and Hashimoto, M., *Surf. Sci.* **171**, L418 (1986); *Shinku (Vacuum)* **28**, 810 (1985). [Japanese]
2. Watanabe, M., and Kadowaki, T., *Appl. Surf. Sci.* **28**, 147 (1987).
3. Bootsma, G. A., and Meyer, F., *Surf. Sci.* **14**, 52 (1969).
4. McIntyre, J. D. E., *in* "Optical Properties of Solids: New Development" (B. O. Seraphin, Ed.), p. 555. North-Holland, Amsterdam, 1976.
5. Aspnes, D. E., *in* "Optical Properties of Solids: New Development" (B. O. Seraphin, Ed.), p. 800. North-Holland, Amsterdam, 1976.
6. McIntyre, J. D. E., and Aspnes, D. E., *Surf. Sci.* **24**, 417 (1971).
7. Pockrand, I., and Otto, A., *Appl. Surf. Sci.* **6**, 362 (1980).
8. Tsang, J. S., Demuth, J. E., Sanda, P. N., and Kirtley, J. R., *Chem. Phys. Lett.* **76**, 54 (1980).
9. Dry, M. E., "Catalysis" (J. R. Anderson, and M. Boudouard, Eds.), Vol. 1, Chap. 4. Springer-Verlag, Berlin/New York, 1981.
10. Reuel, R. C., and Bartholomew, C. H., *J. Catal.* **85**, 78 (1984).
11. Papp, H., *Surf. Sci.* **129**, 205 (1983).
12. Bridge, M. E., Comrie, C. M., and Lambert, R. M., *Surf. Sci.* **67**, 393 (1977).
13. Greuter, F., Heskett, D., Plummer, E, W., and Freund, H. J., *Phys. Rev.* **27**, 7117 (1983).
14. Fu, L., and Bartholomew, C. H., *J. Catal.* **92**, 376 (1985).
15. Steinbach, F., Kiss, J., and Krall, R., *Surf. Sci.* **157**, 401 (1985).
16. Tiscione, P., and Rovida, G., *Surf. Sci.* **154**, L255 (1985).
17. Zowtiak, J. M., and Bartholomew, C. H., *J. Catal.* **83**, 107 (1983).
18. Hauge, P. A., and Dill, F. H., *IBM J. Res. Dev.* **17**, 472 (1973).
19. Habraken, F. H. P. M., Gijzeman, O. L. J., and Bootsma, G. A., *Surf. Sci.* **96**, 482 (1980).
20. Feibelman, P. J., *Prog. Surf. Sci.* **12**, 267 (1982).
21. Abeles, F., and Lopez-Rios, T., *Surf. Sci.* **96**, 32 (1980).
22. Nakamura, J., Toyoshima, I., and Tanaka, Ken., private communication.
23. Watanabe, M., *in* "Thin Metal Films and Gas Chemisorption" (P. Wissmann, Ed.), Chap. 8, p. 369. Elsevier, Amsterdam, 1987.
24. Watanabe, M., and Wissmann, P., *Surf. Sci.* **138**, 95 (1984).
25. Tuinstra, F., and Koenig, J. L., *Phys. Rev.* **53**, 1126 (1970).
26. Elman, B. S., Dresselhaus, M. S., Dresselhaus, G., Maby, E. W., and Mazurek, H., *Phys. Rev. B* **24**, 1027 (1981).
27. Marzouk, H. A., Bradley, E. B., and Arunkumar, K. A., *Spectrosc. Lett.* **18**, 189 (1985).
28. Carroll, J. J., and Melmed, A. J., *Surf. Sci.* **16**, 251 (1969).
29. Watanabe, M., Wedler, G., and Wissmann, P., *Surf. Sci.* **154**, L207 (1985).
30. Speiser, R., *in* "Metal Hydrides" (W. M. Mueller, S. P. Blackledge, and G. G. Libowitz, Eds.), Chap. 3. Academic Press, New York, 1968.
31. Kiuchi, K., and McLellan, R. B., *Acta Metall.* **31**, 961 (1983).
32. Behm, R. J., Penka, V., Cattania, M. G., Christman, K., and Ertl, G., *J. Chem. Phys.* **78**, 7486 (1983).